Materials Research Proceedings 41 (2024) 242-248 https://doi.org/10.21741/9781644903131-27

Corrective capabilities of different rescanning strategies to restore microstructure and density of initially porous 316L laser powder bed fusion

LE SAINT Théo[1,a *], KELLER Clément[1,b], ABROUG Foued[1,c] and ARNAUD Lionel[1,d]

[1]Laboratoire Génie de Production (LGP), Université de Technologie de Tarbes, France

[a]theo.le_saint@uttop.fr, [b]clement.keller@uttop.fr, [c]foued.abroug@uttop.fr, [d]lionel.arnaud@uttop.fr

Keywords: LPBF, Rescanning, 316L, Defects, Microstructure, Characterization

Abstract. Mechanical properties of Laser Power Bed Fusion (LPBF) parts, and particularly fatigue properties, are heavily affected by defects including surface roughness or porosity. To mitigate the occurrence of these defects, in-situ and on-line corrective measures can be implemented to the fabrication process, among them, rescanning, which consists in remelting an already solidified layer. Initially porous LPBF samples were created and then rescanned using different scanning parameters and strategies. Results show that it is possible to regain part's health, compared to a standardly processed one, in terms of density, hardness and even improved roughness. This remelting process is known to refine microstructure of fabricated materials as well as reduce surface roughness and porosity without requiring further post-processing steps. Therefore, employing rescanning as a corrective technique appears to be a promising approach for rectifying detected defects during the fabrication process. The objective of this study is to assess the corrective capabilities of different rescanning strategies to restore the microstructure of an initially porous 316L LPBF simulating a defected part. This study shows that various rescanning strategies allow for densification of initially porous material from 98.83 ± 0.20 % to 99.75 ± 0.09 %, as well as lateral surface roughness reduction from Ra 20.2 ± 5.2 µm to Ra 12.7 ± 0.1 µm and microhardness increase from 243 ± 5 $HV_{0.5}$ to 253 ± 3 $HV_{0.5}$.

Introduction

Laser Powder Bed Fusion (LPBF) is a metallic additive manufacturing process, that consists in selectively melt thin layers of metallic powder on top of each other [1]. This process enables the manufacturing of geometrically complex parts, allowing for weight reduction in structures [2]. The thermal gradients and cooling rate occurring during fabrication produce a complex and often fine microstructure within the materials, leading to enhanced mechanical properties compared to their conventionally produced counterparts, particularly a higher yield strength, ultimate tensile strength and better ductility [3,4]. However, the mechanical properties, and especially the fatigue life, of LPBF parts are heavily affected by the presence of defects. This encompasses surface roughness, residual stress and porosity within the material such as lack of fusion, gas induced porosity or keyholes [5].

Hence, there is a need for corrective actions to mitigate defects, which can be in the form of post-processing steps. Grinding, polishing, milling or media blasting allow for surface roughness reduction [6] but are not applicable for complex geometry. Hot Isostatic Pressing can reduce porosity but coarsen the fine LPBF microstructure [7] and does not entirely eliminate fully enclosed porosity [8].

Another approach is in-situ monitoring of the fabrication through real-time vision, spectral, acoustic or thermal signal acquisition and treatment to either modify the process parameters on the spot with a close-loop control framework [9] or trigger a corrective response such as complete

Materials Research Proceedings 41 (2024) 242-248 https://doi.org/10.21741/9781644903131-27

layer removal [10] or rescanning. This latter process consists in remelting an already solidified layer using the already existing laser, thus requiring no modification of the machine. Rescanning is known to reduce surface roughness [11-13], refine the microstructure features such as grain or sub-grain cell size [14,15], increase tensile properties [16,17] and on top, densify the parts [11,12,14,18]. Some studies have explored rescanning as a corrective action [18,19], nevertheless, the corrective capabilities of various rescanning strategies remain unexplored.

In this study, rescanning as an in-situ corrective response to defects is tested. Initially porous 316L samples are produced, simulating defected parts, and different rescanning strategies and powers are applied. The main objectives of this study are to identify the rescanning parameters best suited to regain the material density and to characterize the effect on the defect population. The impact of this corrective rescan on the surface roughness and microhardness of the sample is also assessed.

Materials and Methods

All the specimens in this study have been fabricated with AISI 316L (LaserForm 316L (B)) produced by 3D Systems. This powder has a granulometric distribution D_{10}, D_{50} and D_{90} of 9.8, 20.1 and 38.1µm respectively. All the samples were produced using a 3D Systems ProX DMP 300B LPBF machine, the standard process parameters for this powder are listed in Table 1.

Table 1: Standard process parameters for 316L on ProX DMP 300.

P [W]	V [mm/s]	Lt [µm]	H [µm]	Ev [J/mm^3]	Rotation angle [°]	Scanning pattern	Contour
215	1800	40	50	59.72	67	Bi-directional	n.a.

To assess the corrective capabilities of rescanning, 10×10×10mm^3 cubes are fabricated with an initial low power scan to favor the apparition of natural defect and then different rescanning powers and strategies are applied. The initial scan is at 80% of the standard power, corresponding to 172W and the subsequent rescanning powers tested are 80%, 100%, 120% and 150% of the standard scanning power, respectively corresponding to 172W, 215W, 258W and 323W. The rescanning strategy is either SR: Superimposed Rescanning or PR: Perpendicular Rescanning, respectively 0° and 90° between the scan and the rescan, as illustrated in Fig. 1a. The nomenclature of the sample is detailed in Fig 1b. In addition, 2 samples are added, called 80 and 100, with only an initial scan of respectively 80% and 100% of scanning power, 80 being the reference sample with no correction rescanning applied and 100 being the standard sample as it is manufactured with standard parameters and thus acting as the correction aim of this study.

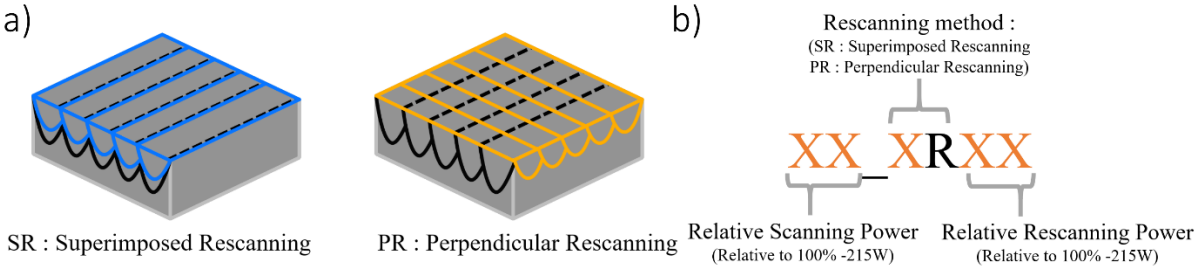

Figure 1: a) Schematics of the rescanning strategies tested in this study and b) nomenclature of the samples.

All the samples were automatically polished using SiC paper up to 4000 grit. Image analysis was employed to determine the density of each sample. The Keyence VHX-5000 optical microscope captured assembly images of the entire samples at ×100 magnification. Each assembly

measured 13.1×11.6 mm, with a resolution of 2.16 µm/pixel, effectively covering the entirety of each sample. Subsequently, the micrographs were segmented using Matlab, allowing for density calculation and defect population characterization, such as defect size distribution. For those data treatments, only defects with an area above 10 pixels are treated.

The lateral surface roughness of the samples was assessed using micrographs of the radial sections of the samples at ×100 magnifications. The images were binarized and the profiles were defined as the sum of the most radially extreme pixels. Allowing to calculate the arithmetic mean Ra and the maximum peak to valley Rz of each sample. For each sample, Ra and Rz values were calculated over two profiles and of all the samples the shortest profile was 4.9 mm long.

To assess the impact of rescanning on mechanical properties, microhardness testing was carried out using a Zwick Roell DuraScan 70. For each sample, 60 HV0.5 indentations were performed in bulk zones of the samples with 0.5 mm spacing over x and y between indents.

Results and discussions

The density of the samples for different rescanning powers and strategies is shown in Fig. 2a. The density exhibited by reference sample 80 (98.83 ± 0.20 %) is rather low compared to the density of the standard sample 100 (99.97 ± 0.01 %). The density evolution with rescanning power is nearly the same for both rescanning strategies. An initial density decrease is noted at 80% of rescanning power with a subsequent regain in density for 100% with a value of 99.75 ± 0.09 % for 80_SR100 (SR: Superimposed Rescanning). Above 100% of rescanning laser power, only a slight increase is noted for 80_SR150 with a density of 99.86 ± 0.02 %.

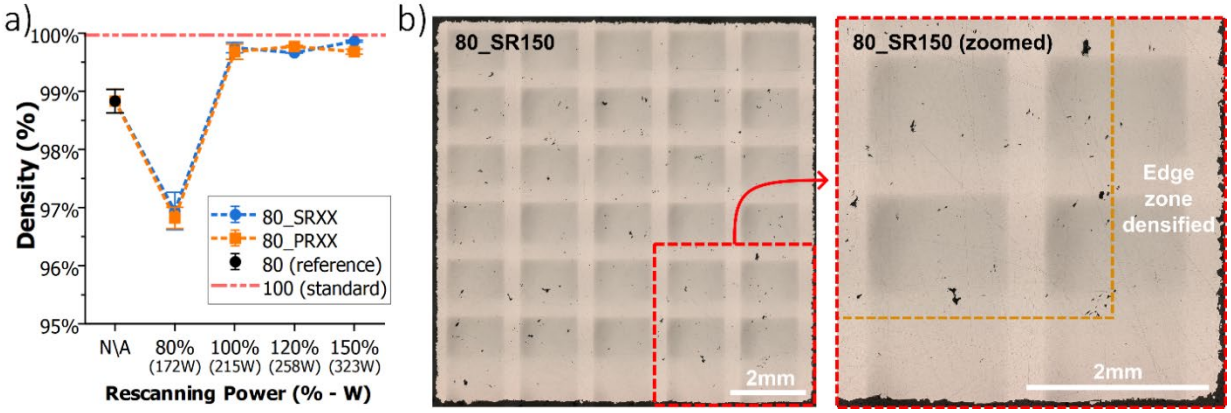

Figure 2: a) Density of samples versus rescanning power for different rescanning strategies, b) micrograph of 80_SR150.

For rescanning powers of 120% and 150%, the edge part of the samples seems denser than the bulk part, as shown in Fig. 2b. This might be explained by the high thermal energy input of above 100% of rescanning power and a reduced thermal conductivity in edge zones compared to bulk zones due to the presence of powder.

When it comes to defect size, the distributions of the maximum Feret diameter of the porosities of the reference sample 80, 80_SR100 and the sample fabricated with standard process parameters 100 are shown in Fig 3, which also shows the total number of defects detected and the maximum Feret diameter of the biggest defect of each sample. Superimposed rescanning with 100% of rescanning power allowed for a decrease in the size of the biggest defect from 350 µm down to 229 µm. This defect size, although reduced, is still significantly bigger than the biggest defect of the standard sample 100, which exposes a biggest defect of 48 µm.

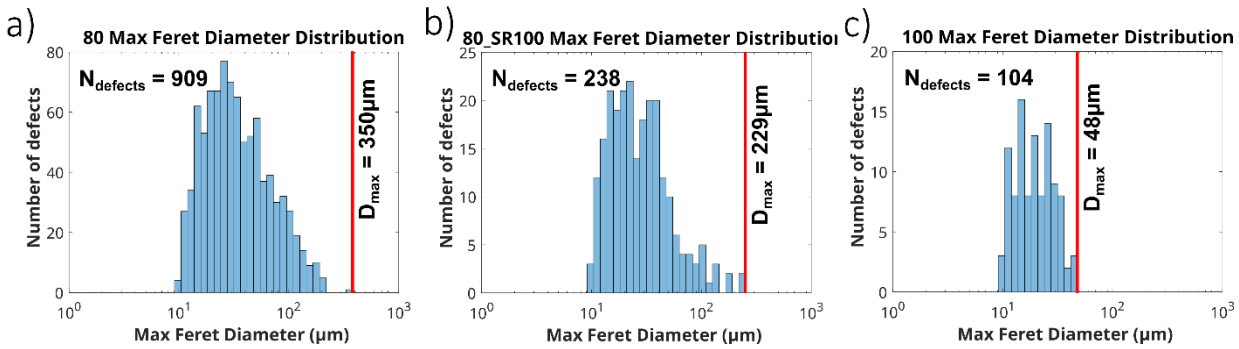

Figure 3: Maximum Feret diameter distribution, number of defects and maximum Feret diameter of the biggest defect of the defect population of a) 80, b) 80_SR100 and c) 100.

Rescanning seems to also significantly decrease the number of defects. For the sample 80_SR100, the number of defects is 3.8 times lower than the reference sample 80. The number of defects present in 80_SR100 remains however 2.3 times higher than the standard sample 100. It can also be noted that the shape of the distribution of defect size is modified between 80 and 80_SR100. Particularly, the right side of the 80_SR100 distribution is lowered, revealing a greater impact of rescanning on the biggest defects of the whole population.

Regarding the surface roughness, the evolution of the lateral values of this parameter, Ra and Rz are shown in respectively Fig. 4a and Fig. 4b, for various rescanning powers and strategies. The reference sample 80 reveals higher lateral surface roughness values of Ra 20.2 ± 5.2 µm and Rz 190 ± 56 µm than the standard sample 100 with values of Ra and Rz of respectively 16.3 ± 1.7 µm and 161 ± 39 µm. With both rescanning strategies at 80% of rescanning power, the surface roughness is even higher. For all samples rescanned with 100% of rescanning power or above, except for the sample 80_SR120, Ra and Rz values are reduced compared to the reference sample 80, with a minimum reached at Ra 12.7 ± 0.1 µm and Rz 108 ± 6 µm for 80_PR120 (PR: Perpendicular Rescanning). It is worth mentioning that 80_SR150, 80_PR120 and 80_PR150 expose lateral roughness values even below the standard sample 100 ranges, meaning that rescanning might also be used to improve lateral surface roughness.

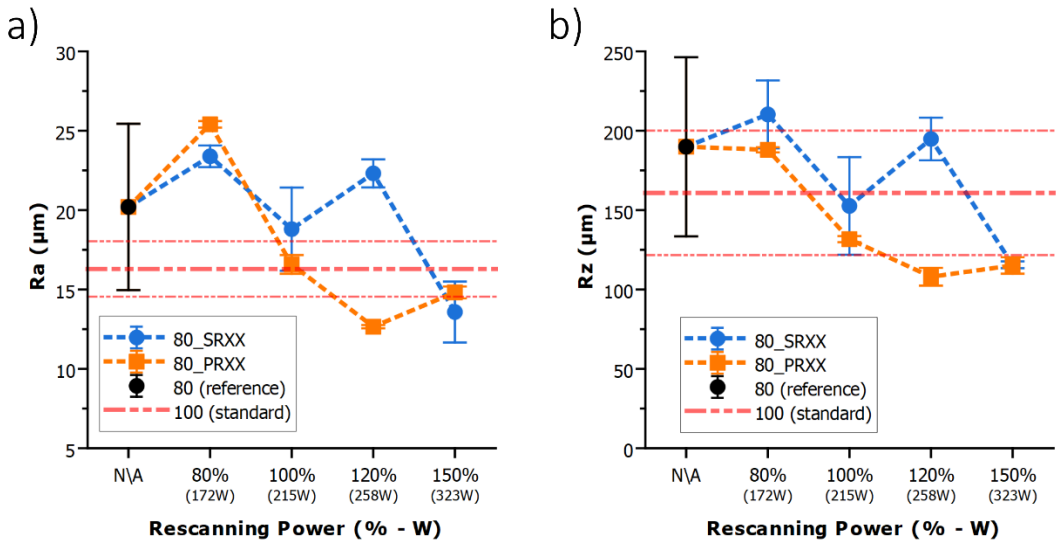

Figure 4: Lateral surface roughness a) Ra and b) Rz of samples versus rescanning power for different rescanning strategies.

Finally, to assess the regain in mechanical properties along with densification, the samples are submitted to HV0.5 microhardness testing. The reference sample 80 exhibits a microhardness of 243 ± 5 $HV_{0.5}$, lower than for the standard sample 100 with a value of 254 ± 2 $HV_{0.5}$. Both rescanning strategies show a microhardness maximum for 100% of rescanning power with value for 80_SR100 and 80_PR100 respectively being 253 ± 3 $HV_{0.5}$ and 252 ± 1 $HV_{0.5}$. Those values are fairly equivalent to the one of the reference 100 sample. All other rescanned samples exhibit microhardness lower than the reference.

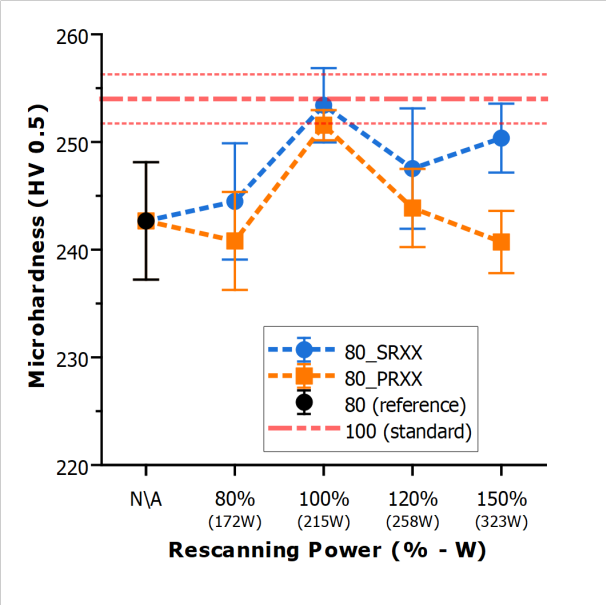

Figure 5: HV0.5 microhardness versus rescanning power for different rescanning strategies.

Considering all the characterization performed in this study, it seems that laser power during rescanning must be equivalent to the one of the first laser scan to recover as much as possible the material properties of defected layers in LPBF process.

Conclusions

Results show that rescanning as a defect correction measure is promising. The main findings of the study are as follows:

- Most of the density, surface roughness and microhardness are restored with superimposed rescanning at 100% of scanning power compared to the standard material. Particularly, between samples 80 and 80_SR100, the density is increased from 98.83 ± 0.20 % to 99.75 ± 0.09 % as well as the microhardness from 243 ± 5 $HV_{0.5}$ to 253 ± 3 $HV_{0.5}$ and the surface roughness is reduced from of Ra 20.2 ± 5.2 µm and Rz 190 ± 56 µm to Ra 18.8 ± 2.6 µm and Rz 153 ± 31 µm.
- Superimposed rescanning at 150% leads to even better density of 99.86 ± 0.02 % compared to superimposed rescanning at 100% as well as reduction in lateral surface roughness compared to the standard material. Indeed, 80_SR150 exposes lateral roughness of Ra 13.2 ± 1.9 µm and Rz 116 ± 2 µm, lower than the standard material 100 with Ra 16.3 ± 1.7 µm and 161 ± 39 µm. However, the microhardness is no fully restored.
- Superimposed or perpendicular rescanning strategies show similar results, with superimposed strategy being slightly better to restore materials properties.

References

[1] W. E. Frazier, « Metal Additive Manufacturing: A Review », *J. of Materi Eng and Perform*, vol. 23, nº 6, p. 1917-1928, juin 2014. https://doi.org/10.1007/s11665-014-0958-z

[2] G. Schuh, G. Bergweiler, K. Lichtenthäler, F. Fiedler, et S. de la Puente Rebollo, « Topology Optimisation and Metal Based Additive Manufacturing of Welding Jig Elements », *Procedia CIRP*, vol. 93, p. 62-67, janv. 2020. https://doi.org/10.1016/j.procir.2020.04.066

[3] Y. M. Wang *et al.*, « Additively manufactured hierarchical stainless steels with high strength and ductility », *Nature Mater*, vol. 17, nº 1, Art. nº 1, janv. 2018. https://doi.org/10.1038/nmat5021

[4] L. Liu *et al.*, « Dislocation network in additive manufactured steel breaks strength–ductility trade-off », *Materials Today*, vol. 21, nº 4, p. 354-361, mai 2018. https://doi.org/10.1016/j.mattod.2017.11.004

[5] S. Chowdhury *et al.*, « Laser powder bed fusion: a state-of-the-art review of the technology, materials, properties & defects, and numerical modelling », *Journal of Materials Research and Technology*, vol. 20, p. 2109-2172, sept. 2022. https://doi.org/10.1016/j.jmrt.2022.07.121

[6] H. M. Khan, Y. Karabulut, O. Kitay, Y. Kaynak, et I. S. Jawahir, « Influence of the post-processing operations on surface integrity of metal components produced by laser powder bed fusion additive manufacturing: a review », *Machining Science and Technology*, vol. 25, nº 1, p. 118-176, déc. 2020. https://doi.org/10.1080/10910344.2020.1855649

[7] I. S. Grech, J. H. Sullivan, R. J. Lancaster, J. Plummer, et N. P. Lavery, « The optimisation of hot isostatic pressing treatments for enhanced mechanical and corrosion performance of stainless steel 316L produced by laser powder bed fusion », *Additive Manufacturing*, vol. 58, p. 103072, oct. 2022. https://doi.org/10.1016/j.addma.2022.103072

[8] S. Tammas-Williams, P. J. Withers, I. Todd, et P. B. Prangnell, « Porosity regrowth during heat treatment of hot isostatically pressed additively manufactured titanium components », *Scripta Materialia*, vol. 122, p. 72-76, sept. 2016. https://doi.org/10.1016/j.scriptamat.2016.05.002

[9] Y. Cai, J. Xiong, H. Chen, et G. Zhang, « A review of in-situ monitoring and process control system in metal-based laser additive manufacturing », *Journal of Manufacturing Systems*, vol. 70, p. 309-326, oct. 2023. https://doi.org/10.1016/j.jmsy.2023.07.018

[10] B. M. Colosimo, E. Grossi, F. Caltanissetta, et M. Grasso, « Penelope: A Novel Prototype for In Situ Defect Removal in LPBF », *JOM*, vol. 72, nº 3, p. 1332-1339, mars 2020. https://doi.org/10.1007/s11837-019-03964-0

[11] B. Liu, B.-Q. Li, et Z. Li, « Selective laser remelting of an additive layer manufacturing process on AlSi10Mg », *Results in Physics*, vol. 12, p. 982-988, mars 2019. https://doi.org/10.1016/j.rinp.2018.12.018

[12] W. Yu, S. L. Sing, C. K. Chua, et X. Tian, « Influence of re-melting on surface roughness and porosity of AlSi10Mg parts fabricated by selective laser melting », *Journal of Alloys and Compounds*, vol. 792, p. 574-581, juill. 2019. https://doi.org/10.1016/j.jallcom.2019.04.017

[13] J.-P. Kruth, M. Badrossamay, E. Yasa, J. Deckers, L. Thijs, et J. Humbeeck, « Part and material properties in selective laser melting of metals », *16th International Symposium on Electromachining, ISEM 2010*, janv. 2010.

[14] A. Liang, K. S. Pey, T. Polcar, et A. R. Hamilton, « Effects of rescanning parameters on densification and microstructural refinement of 316L stainless steel fabricated by laser powder bed fusion », *Journal of Materials Processing Technology*, vol. 302, p. 117493, avr. 2022. https://doi.org/10.1016/j.jmatprotec.2022.117493

[15] S. Griffiths, M. D. Rossell, J. Croteau, N. Q. Vo, D. C. Dunand, et C. Leinenbach, « Effect of laser rescanning on the grain microstructure of a selective laser melted Al-Mg-Zr alloy »,

Materials Characterization, vol. 143, p. 34-42, sept. 2018. https://doi.org/10.1016/j.matchar.2018.03.033

[16] C. Keller, M. Mokhtari, B. Vieille, H. Briatta, et P. Bernard, « Influence of a rescanning strategy with different laser powers on the microstructure and mechanical properties of Hastelloy X elaborated by powder bed fusion », *Materials Science and Engineering: A*, vol. 803, p. 140474, janv. 2021. https://doi.org/10.1016/j.msea.2020.140474

[17] T. Han *et al.*, « Refined microstructure and enhanced mechanical properties of AlCrFe2Ni2 medium entropy alloy produced via laser remelting », *Journal of Materials Science & Technology*, vol. 99, p. 18-27, févr. 2022. https://doi.org/10.1016/j.jmst.2021.05.033

[18] E. Yasa et J.-P. Kruth, « Microstructural investigation of Selective Laser Melting 316L stainless steel parts exposed to laser re-melting », *Procedia Engineering*, vol. 19, p. 389-395, janv. 2011. https://doi.org/10.1016/j.proeng.2011.11.130

[19] J. Mireles, S. Ridwan, P. Morton, A. Hinojos, et R. Wicker, « Analysis and correction of defects within parts fabricated using powder bed fusion technology », *Surface Topography: Metrology and Properties*, vol. 3, p. 034002, août 2015. https://doi.org/10.1088/2051-672X/3/3/034002

[20] B. Shen *et al.*, « Influence of laser post-processing on pore evolution of Ti–6Al–4V alloy by laser powder bed fusion », *Journal of Alloys and Compounds*, vol. 818, p. 152845, mars 2020. https://doi.org/10.1016/j.jallcom.2019.152845